Modelling of UAV Formation Flight using 3D Potential Field

Tobias Paul [a], Thomas R. Krogstad [b], Jan Tommy Gravdahl [b,*]

[a] *ESG Elektroniksystem- und Logistik GmbH, Fürstenfeldbruck, Germany*

[b] *Department of Engineering Cybernetics, Norwegian University of Science and Technology, Trondheim, Norway*

Abstract

In this paper we present a solution for formation flight and formation reconfiguration of unmanned aerial vehicles (UAVs). Based on a virtual leader approach, combined with an extended local potential field, the method is universal applicable by driving the vehicle's auto pilot. The solution is verified, using a group of UAVs based on a simplified small-scale helicopter, which is simulated in MATLAB™/Simulink™. As necessary for helicopters, the potential field approach is realized in 3D including obstacle and collision avoidance. The collision avoidance strategy could be used separately for the *sense and avoid* problem.

Key words: Unmanned systems, aerospace control, modelling, collision avoidance, formation flight

1 Introduction

The contribution of this paper is the presentation of a virtual leader formation approach combined with an extended version of the potential field solution presented in [1] and [2]. The approach is applied to a formation of helicopter UAVs presented in [3], providing obstacle and collision avoidance. The helicopters are of the traditional main rotor - tail rotor type. The algorithm supports flight with maximum vehicle speed and could be adopted easily to vehicles with different dynamics. To the authors knowledge, a potential field

* Corresponding author.
Email addresses: tobias.paul@esg.de (Tobias Paul), thomas.krogstad@itk.ntnu.no (Thomas R. Krogstad), tommy.gravdahl@itk.ntnu.no (Jan Tommy Gravdahl).

approach has not previously been applied on helicopter UAVs. However, a two dimensional approach for marine vehicles is presented in [1] while [2] presents a solution for tricycles.

Modelling and control of formations of UAVs is a large and ever increasing field of research. Other formation flight approaches, focusing on fixed wing aircrafts, can be found in [4], [5] or [7]. In [14], control of a formation of fixed winged aircraft taking off and landing on a ship is studied. Control of a formation of a piloted aircraft in formation with an UAV was reported in [6], while [15] report formation flight of three miniature jet aircraft.

UAVs are small size, light weight, able to operate autonomously and also be replaced at low cost. With these qualities, UAVs are interesting for industrial and military purposes. UAVs have been used for mapping of hot spots during forest fires [8] or agricultural and crop monitoring [9]. There is also a wide field of military applications. Applications are, among others, surveillance, reconnaissance, radio jamming, artillery acquisition, and target simulation. Formations of UAVs can distribute the equipment, necessary for a specific mission, to all vehicles in the swarm and offer a huge increase of performance and robustness compared to a single operating vehicle.

The two main approaches for formation control are potential field and leader-follower. Combinations of those two approaches are often used to build and move formations because they are effective, robust and easy to handle [2], [1].

As UAVs, helicopters are of special interest. They are able to perform vertical take-offs and landings (VTOL) and to hover. Helicopters can operate from ships, undeveloped, or urban areas. Modeling and control of helicopters is challenging because of varying flight qualities and coupling of the dynamic equations. Nevertheless, in [10] and [11] one can find two nonlinear models for full scale helicopters. Especially small scale helicopter are interesting for UAV applications. They have a very high thrust to weight ratio and can perform extreme maneuvers. A complete and very detailed mathematical model of a small scale helicopter is presented by [12]. A classical control approach is based on a cascade controller, controlling attitude in the inner, lateral and longitudinal movement in the outer loop [3]. Other approaches are based on solving the state dependent Riccati equation [13] or neural networks [16].

2 Modelling

The helicopter is modeled as a rigid body using a north-east-down (NED, labeled by $\cdot^n$) and a body fixed reference frame (labeled by $\cdot^b$). The NED position is given by

$$\mathbf{p}^n = \begin{bmatrix} x & y & z \end{bmatrix}^T$$

with x pointing to true North, y pointing East, and z pointing downwards. The vehicles attitude is described by Euler angles

$$\mathbf{\Theta} = \begin{bmatrix} \phi & \theta & \psi \end{bmatrix}^T, \tag{1}$$

with pitch angle ϕ, roll angle θ, and yaw angle ψ. Velocities are described in a body fixed frame with linear velocity

$$\mathbf{v}^b = \begin{bmatrix} u & v & w \end{bmatrix}^T. \tag{2}$$

The velocity u points from aft to fore, v to starboard, and w from top to bottom. The vector

$$\boldsymbol{\omega}^b = \begin{bmatrix} p & q & r \end{bmatrix}^T \tag{3}$$

is the angular velocity of the body fixed frame relative to the NED frame, decomposed in the body fixed frame. Finally,

$$\boldsymbol{\nu} = \begin{bmatrix} \mathbf{v}^b & \boldsymbol{\omega}^b \end{bmatrix}^T \text{ and} \tag{4}$$

$$\boldsymbol{\eta} = \begin{bmatrix} \mathbf{p}^n & \mathbf{\Theta} \end{bmatrix}^T \tag{5}$$

combine the vectors of the two reference frames and form together with the main rotor speed Ω_{mr} and the blade flapping angles a_1 and b_1 (see Fig. 1) the states $\mathbf{x}$ of the helicopter according to

$$\mathbf{x} = \begin{bmatrix} \boldsymbol{\nu}^T & \boldsymbol{\eta}^T & a_1 & b_1 & \Omega_{mr} \end{bmatrix}^T. \tag{6}$$

The kinematic equation for a six degree of freedom vehicle is given by [17] as

Fig. 1. Body fixed frame and helicopter components

$$\dot{\boldsymbol{\eta}} = \begin{bmatrix} \mathbf{R}_b^n(\mathbf{\Theta}) & \mathbf{0}_{3\times3} \\ \mathbf{0}_{3\times3} & \mathbf{T}_{\mathbf{\Theta}}(\mathbf{\Theta}) \end{bmatrix} \boldsymbol{\nu}, \tag{7}$$

using the rotation matrix

$$\mathbf{R}_b^n(\mathbf{\Theta}) = \begin{bmatrix} c_\psi c_\theta & c_\psi s_\theta s_\phi - s_\psi c_\phi & s_\psi s_\phi + c_\psi c_\phi s_\theta \\ s_\psi c_\theta & c_\psi c_\phi + s_\phi s_\theta s_\psi & s_\theta s_\psi c_\phi - c_\psi s_\phi \\ -s_\theta & c_\theta s_\phi & c_\theta c_\phi \end{bmatrix}, \tag{8}$$

and the kinematic transformation matrix

$$\mathbf{T}_{\mathbf{\Theta}}(\mathbf{\Theta}) = \begin{bmatrix} 1 & s_\phi t_\theta & c_\phi t_\theta \\ 0 & c_\phi & -s_\phi \\ 0 & s_\phi / c_\theta & c_\phi / c_\theta \end{bmatrix}, \tag{9}$$

with $s. \equiv \sin(\cdot)$, $c. \equiv \cos(\cdot)$, and $t. \equiv \tan(\cdot)$. Using Euler angles restricts the vehicle's roll angle to $-90^\text{o} < \theta < 90^\text{o}$ due to the singularities in equation (9). This could have been avoided using quaterions, but Euler angels are used due to a more straightforward interpretation of the results. The blades can be rotated around their length to control the helicopter movement. Lift is controlled by rotation of all blades at the same time (collective) and attitude by inducing an angle depending on the blade position (cyclic). Doing this, the blade angle performs a sinusoidal curve during one round affecting the attitude and leading to a course change. The control inputs given by

$$\mathbf{u} = \begin{bmatrix} \delta_{col} & \delta_{lon} & \delta_{lat} & \delta_r & \delta_t \end{bmatrix}^T, \tag{10}$$

are equal to those a pilot uses. Here, δ_{col} is the collective control input for the collective pitch of the main rotor blades given in rad, δ_{lon} and δ_{lat} are the cyclic control inputs giving the explicit pitch in longitudinal and lateral direction, δ_r is the collective pitch for the tail rotor, where no cyclic pitch is necessary. Finally, δ_t is the engine control input to keep the rotor speed constant and varies between 0 and 1.

2.1 Rigid body dynamics

The equations of motion will be presented using the notation of [17]:

$$\mathbf{M}_{RB}\dot{\boldsymbol{\nu}} + \mathbf{C}_{RB}(\boldsymbol{\nu})\boldsymbol{\nu} = \boldsymbol{\tau}(\mathbf{u}). \tag{11}$$

Here, $\mathbf{M}_{RB}$ is the system inertia matrix, $\mathbf{C}_{RB}(\boldsymbol{\nu})$ the coriolis-centripetal matrix, and $\boldsymbol{\tau}$ a vector of forces and moments caused by aerodynamics, gravity

and engine. $\mathbf{M}_{RB}$ has a very simple form because of neglecting the cross-axis moments of inertia due to the fact that the origin of the body frame is placed in the helicopter's center of gravity while rotational symmetry is assumed [12], [18]. Doing so, $\mathbf{M}_{RB}$ is given by

$$\mathbf{M}_{\mathrm{RB}} = \begin{bmatrix} \mathrm{m}\mathbf{I}_{3\times3} & \mathbf{0}_{3\times3} \\ \mathbf{0}_{3\times3} & \mathbf{I}_0 \end{bmatrix}. \tag{12}$$

Here, $\mathbf{I}_{3\times3}$ is a unity matrix, $\mathbf{I}_0$ the system inertia matrix and m the helicopter's mass. The matrix $\mathbf{C}_{RB}$ can be realized in different ways. In [17], Kirchoff's equations were used to derive an explicit expression. Because

$$\mathbf{M}_{RB} = \mathbf{M}_{RB}^T = \begin{bmatrix} \mathbf{M}_{11} & \mathbf{0}_{3\times3} \\ \mathbf{0}_{3\times3} & \mathbf{M}_{22} \end{bmatrix} \tag{13}$$

holds, $\mathbf{C}_{RB}$ can be build up from the elements of $\mathbf{M}_{RB}$ according to

$$\mathbf{C}_{RB}(\boldsymbol{\nu}) = \begin{bmatrix} \mathbf{0}_{3\times3} & -S(\mathbf{M}_{11}\boldsymbol{\nu}_1) \\ -S(\mathbf{M}_{11}\boldsymbol{\nu}_1) & -S(\mathbf{M}_{22}\boldsymbol{\nu}_2) \end{bmatrix} \tag{14}$$

using the vector cross product operator $S(\cdot)$, defined as

$$\boldsymbol{\lambda} \times \mathbf{a} := S(\boldsymbol{\lambda})\mathbf{a}, \tag{15}$$

where $\boldsymbol{\lambda}$, $\mathbf{a} \in \mathbb{R}^3$ and $S(\cdot)$ is defined as

$$S(\boldsymbol{\lambda}) = -S(\boldsymbol{\lambda})^T = \begin{bmatrix} 0 & -\lambda_3 & \lambda_2 \\ \lambda_3 & 0 & -\lambda_1 \\ -\lambda_2 & \lambda_1 & 0 \end{bmatrix}. \tag{16}$$

2.2 Forces and moments

A complex model of a small scale helicopter is presented in [12] including all parameter values. The modeled forces and moments $\boldsymbol{\tau} = \begin{bmatrix} \mathbf{f}_o^b & \mathbf{m}_o^b \end{bmatrix}^T$, decomposed in body frame are given by

$$\mathbf{f}_o^b = \begin{bmatrix} X_{mr} + X_{fus} \\ Y_{mr} + Y_{fus} + Y_{tr} + Y_{vf} \\ Z_{mr} + Z_{fus} + Z_{ht} \end{bmatrix} + \mathbf{f}_g^b, \tag{17}$$

$$\mathbf{m}_o^b = \begin{bmatrix} L_{mr} + L_{vf} + L_{tr} \\ M_{mr} + M_{ht} \\ -Q_e + N_{vf} + N_{tr} \end{bmatrix}. \tag{18}$$

The indexes represent the causing component which can be found in Fig. 1. Gravity decomposed in the body frame is given by

$$\mathbf{f}_g^b = \mathbf{R}_b^n(\mathbf{\Theta})^T \begin{bmatrix} 0 \\ 0 \\ \mathrm{mg} \end{bmatrix} \tag{19}$$

while Q_e represents the engine torque. The main rotor dominates vertical, pitch and roll dynamic, while the tail rotor dominates the yaw dynamic. The main rotor forces and moments are caused by the thrust T_{mr}. As shown in [10], an iterative approach is necessary to calculate it. In addition, control is complicated because of coupling between the control inputs. Because of those issues, the full model of the small-scale helicopter is difficult to control and to simulate. As our formation control approach is independent of the underlying dynamics, provided hover and vertical flight is possible, we choose the simplified model in [3] for simulations. Using this model, the force representation change to:

$$\mathbf{f}_o^b = \begin{bmatrix} 0 \\ 0 \\ Z_{mr} \end{bmatrix} + \mathbf{f}_g^b, \tag{20}$$

$$\mathbf{m}_o^b = \begin{bmatrix} L_{mr} \\ M_{mr} \\ N_{mr} \end{bmatrix} + \begin{bmatrix} Y_{mr}\mathrm{h_{mr}} + Y_{tr}\mathrm{h_{tr}} \\ -X_{mr}\mathrm{h_{mr}} \\ -Y_{tr}\mathrm{l_{tr}} \end{bmatrix}, \tag{21}$$

where h_{mr} represents the vertical distance from main rotor to the center of gravity and l_{tr} the horizontal distance of the tail rotor. The components in (20) and (21) are modeled in [3] as follows:

$$X_{mr} = -T_{mr}\delta_{lon}, \tag{22}$$
$$Y_{mr} = -T_{mr}\delta_{lat}, \tag{23}$$
$$Z_{mr} = -T_{mr}, \tag{24}$$
$$Y_{tr} = -T_{tr}, \tag{25}$$
$$L_{mr} = \mathrm{c}_{\mathrm{M}}^{\mathrm{Q,T}}\delta_{lat} - \frac{\mathrm{P}_{\max}\delta_t}{\Omega_{mr}}\delta_{lon}, \tag{26}$$
$$M_{mr} = \mathrm{c}_{\mathrm{M}}^{\mathrm{Q,T}}\delta_{lon} + \frac{\mathrm{P}_{\max}\delta_t}{\Omega_{mr}}\delta_{lat}, \text{ and} \tag{27}$$
$$N_{mr} = -\frac{\mathrm{P}_{\max}\delta_t}{\Omega_{mr}}, \tag{28}$$

where $\mathrm{c}_{\mathrm{M}}^{\mathrm{Q,T}}$, $\mathrm{c}_{\mathrm{M}}^{\mathrm{Q,T}}$, and $\mathrm{P}_{\max}$ are constants. The thrusts T_{mr} and T_{tr} are linearized in [3] to

$$T_{mr} = \mathrm{K}_{\mathrm{T_M}}\Omega_{mr}^2\delta_{col} \text{ and} \tag{29}$$
$$T_{tr} = \mathrm{K}_{\mathrm{T_T}}\Omega_{mr}^2\delta_r, \tag{30}$$

where $\mathrm{K}_{\mathrm{T_M}}$ and $\mathrm{K}_{\mathrm{T_T}}$ are constants. The engine dynamics are given by

$$\dot{\Omega}_{mr} = \frac{1}{\mathrm{I}_{\mathrm{rot}}}\left(Q_e - Q_{mr}\right), \tag{31}$$

where the engine torque Q_e is modeled as

$$Q_e = \frac{\mathrm{P}_{\mathrm{e}}^{\max}\delta_t}{\Omega_{mr}} \tag{32}$$

with the constant $\mathrm{P}_{\mathrm{e}}^{\max}$. The torque Q_{mr}, caused by the aerodynamic resistance of the rotor, is modeled as

$$Q_{mr} = \left(\mathrm{c} + \mathrm{d}\delta_{col}^2\right)\Omega_{mr}^2, \tag{33}$$

where c and d are constant. The values of the constants are given in [3]. Fuselage, vertical fin and horizontal tail are not modeled. The main rotor force in direction of u is neglected due to the fact that longitudinal and lateral movement of a helicopters are dominated by the attitude. It is assumed that $Y_{mr} + Y_{tr} = 0$. The controller used with the model is based on a vertical controller and a cascade controller. The cascade controller controls the attitude in the inner loop and the longitudinal and lateral movement in the outer loop. All necessary parameters are included in [3].

3 Formation control

The approach presented in the following generates for each vehicle a potential field depending on swarm constellation, formation, desired, and actual position. It is a combination of virtual leader and potential field approach. A movement of the virtual leader results in a deflection from the desired position and causes the affected vehicles to correct their positions. The field is finally used for obstacle and collision avoidance. A specific position can be assigned to a specific vehicle in the formation. We give an overview of the system in Fig. 2. The advantage of this approach, compared to other approaches, is the application in three dimensions. In addition, a continuous field and thus a continuous trajectory for each vehicle is guaranteed, while providing obstacle and collision avoidance. The algorithm creates a vector which is used to guide the single vehicles. Finally, it guarantees acceleration to maximum vehicle speed. The potential field of each vehicle consists of four components: virtual leader

Fig. 2. Vehicle block diagram

($\mathbf{F}_{vl}$), inter vehicle ($\mathbf{F}_{ij}^{tot}$), collision ($\mathbf{F}_{ca}^{tot}$), and obstacle avoidance ($\mathbf{F}_{oa}^{tot}$). The total field is given by:

$$\tilde{\mathbf{F}}_i^{tot} = \mathbf{F}_{vl} + \mathbf{F}_{ij}^{tot} + \mathbf{F}_{ca}^{tot} + \mathbf{F}_{oa}^{tot}. \tag{34}$$

3.1 Virtual leader

The virtual leader is the anchor of each formation and controls the formation movement. Depending on the underlying control system its trajectory can either be given as waypoints or as a continuous trajectory. The virtual leader's part of the local time dependent potential field is:

$$\mathbf{F}_{vl} = \mathrm{K_{vl}} \left(\mathbf{p}_{vl}^n - \mathbf{p}_i^n - \left[\mathbf{p}_{vl}^n - \mathbf{p}_{i_0}^n \right] \right) \tag{35}$$

$$= \mathrm{K_{vl}} \left(\mathbf{d}_i - \mathbf{d}_{i_0} \right) \tag{36}$$

$\mathrm{K_{vl}}$ is a gain which needs to be tuned. The physical meaning of the variables are illustrated in Fig. 3. The virtual leader component guides the vehicles

Fig. 3. Vector definitions for formation flight; $\mathbf{p}_{vl}^n$: position vector of virtual leader; $\mathbf{p}_i^n$: current position vector of vehicle i; $\mathbf{p}_{i_0}^n$: vehicle i's place in the formation

directly to their desired positions relative to the virtual leader.

3.2 Inter vehicle influence

The contribution of another vehicle to the potential field is expressed by:

$$\mathbf{F}_{ij} = \mathrm{K_{ij}} \left(\mathbf{p}_j^n - \mathbf{p}_i^n - \left[\mathbf{p}_{j_0}^n - \mathbf{p}_{i_0}^n \right] \right) \tag{37}$$

$$= \mathrm{K_{ij}} \left(\mathbf{d}_{ij} - \mathbf{d}_{ij_0} \right) \tag{38}$$

Similar to equations (35) and (36), $\mathbf{p}_j^n$ is the position vector for vehicle j and $\mathbf{p}_{j_0}^n$ is the position vector pointing to vehicle j's position in the formation. $\mathrm{K_{ij}}$ is the inter vehicle gain which needs to be tuned. In a swarm of N vehicles the total component for vehicle i is given by

$$\mathbf{F}_{ij}^{tot} = \sum_{j=1}^{\mathrm{N}} \mathbf{F}_{ij}(i,j) \text{ for } j \neq i. \tag{39}$$

This component preserves the formation by affecting the vehicles to keep the desired distances among themselves. Therefore, the ratio of $\mathrm{K_{vl}}$ and $\mathrm{K_{ij}}$ causes the vehicles to follow the virtual leader (even if the formation breaks) or to preserve their desired formation.

3.3 Collision and obstacle avoidance

To avoid collision between vehicles or obstacles a safety space is defined around each vehicle. Due to simplicity, it is defined as a sphere with positive radius r_{sav}. If necessary, ellipsoids or more complex shapes could be chosen in order to cover the physical appearance of the vehicle in a better way. Tests have been performed using an ellipsoid space. By adding a small pitch angle to the ellipsoid, the vehicle should be supported in ascending or descending while avoiding a collision. This should be realized using the surface of the sphere as a reflection surface.

Nevertheless, using the simplified model, the additional calculation costs do not justify the advantage compared to the sphere. An additional field component is generated if something enters the sphere, pointing away from the invading vehicle or obstacle. To ensure collision avoidance the additional component converges toward infinity in the center of the sphere. The additional field component for vehicle i whose safety sphere is invaded by vehicle j is defined by

$$\mathbf{F}_{ca}^{ij} = \begin{cases} \left(\frac{\mathrm{K_{ca}} r_{sav}}{||\mathbf{d}_{ji}||} - \mathrm{K_{ca}}\right) \frac{\mathbf{d}_{ji}}{||\mathbf{d}_{ji}||} & \text{for } ||\mathbf{d}_{ji}|| < r_{sav} \\ 0 & \text{otherwise} \end{cases}, \tag{40}$$

where $||\cdot||$ represents the vector 2-norm defined as $||\mathbf{x}|| := \sqrt{x_1^2 + x_2^2 + \cdots + x_n^2}$. Furthermore $\mathbf{d}_{ji} = \mathbf{p}_i^n - \mathbf{p}_j^n$. Assuming a destruction free flight, the distance $||\mathbf{d}_{ji}||$ will be always nonzero. With $||\mathbf{d}_{ji}|| = r_{sav}$ equation (40) becomes zero. This allows a smooth insertion of the collision avoidance component and guarantees a continuous potential field. Again, $\mathrm{K_{ca}}$ is a gain which needs to be tuned. The total amount of the collision avoidance term is given by

$$\mathbf{F}_{ca}^{tot} = \sum_{j=1}^{\mathrm{N}} \mathbf{F}_{ca}^{ij} \text{ for } i \neq j. \tag{41}$$

Equation (40) can be expanded on every object. Modeling obstacles as a set of points, compared to the knots in a grid, each point can be treated like vehicles in the swarm. Equation (40) and (41) change to

$$\mathbf{F}_{oa}^{ik} = \begin{cases} \left(\frac{\mathrm{K_{oa}}}{||\mathbf{d}_{ki}||} - \frac{\mathrm{K_{oa}}}{r_{sav}}\right) \frac{\mathbf{d}_{ki}}{||\mathbf{d}_{ki}||} & \text{for } ||\mathbf{d}_{ki}|| < r_{sav} \\ 0 & \text{otherwise} \end{cases} \tag{42}$$

$$\mathbf{F}_{oa}^{tot} = \sum_{k=1}^{\mathrm{M}} \mathbf{F}_{oa}^{ik} \text{ for } i \neq k \tag{43}$$

for obstacle avoidance. Here, $\mathbf{d}_{ki}$ represents one of the M place vectors which model a detected obstacle. The distance between the place vectors should not be larger than $r_{sav}/2$ to provide a complete obstacle recognition for the avoidance. For increased performance, r_{sav} should be chosen dynamically, depending on the vehicle's velocity:

$$r_{sav} = r_{sav}^{min} + \mathrm{K_{sav}} ||\dot{\mathbf{p}}^n||, \tag{44}$$

using $\mathrm{K_{sav}}$ as a gain and r_{sav}^{min} as the minimum distance for a save avoidance. Other choices for (44) are possible.

3.4 Potential field

Summation of the field components gives the magnitude and direction of the potential field for vehicle i at its current position. The field is continuous and singularity free, assuming the restrictions given before. Note that a benefit of this approach is that no knowledge of the UAV model is needed in order

to formulate the various components of the field. It is reasonable to define a maximum amplitude for the force vector while keeping its direction:

$$\mathbf{F}_i^{tot} = \min \left\{ ||\tilde{\mathbf{F}}_i^{tot}||,\ F_{max} \right\} \frac{\tilde{\mathbf{F}}_i^{tot}}{||\tilde{\mathbf{F}}_i^{tot}||} \tag{45}$$

F_{max} will be the upper limit of the field's strength and therefore a limitation for the vehicle's speed. F_{max} should be chosen dynamically to use the maximum vehicle speed. This can be realized by taking the vehicle's NED velocity $||\dot{\mathbf{p}}^n||$ into account:

$$F_{max} = F_{min} + \mathrm{K_v}||\dot{\mathbf{p}}^n|| \tag{46}$$

where F_{min} is a minimum value for F_{max} and $\mathrm{K_v}$ is a gain. As long as the vehicle is accelerating, the distance to the vehicle's reference position will also increase. This keeps the vehicle accelerating until the maximal velocity is reached. Fig. 4 shows a computed potential field for a specific vehicle interacting with two other vehicles. The reference (index r) trajectory $\mathbf{x}_r$ in Fig. 2, which is used

(a)

(b)

Fig. 4. (a) Potential field magnitude (b) Potential field direction.
The used r_{sav} is indicated by black circles and the vehicles position by the red (opponent) and green (desired) lines resp. crosses.

by the controller to calculate the helicopter's control inputs, is based on the desired NED movement

$$\mathbf{p}_{i,r}^n = \mathbf{p}_i^n + \mathbf{F}_i^{tot}. \tag{47}$$

The attitude reference is calculated following [3] by using the NED acceleration as follows

$$\mathbf{a}_r^n = \ddot{\mathbf{p}}_{i,r}^n - \begin{bmatrix} 0 \\ 0 \\ \mathrm{g} \end{bmatrix}, \tag{48}$$

$$\mathbf{n} = \begin{bmatrix} n_x \\ n_y \\ n_z \end{bmatrix} = \frac{\mathbf{a}_r^n}{||\mathbf{a}_r^n||}, \tag{49}$$

$$\theta_r = \mathrm{atan2}\left(-s_{\psi_r} n_y + c_{\psi_r} n_x, n_z\right), \tag{50}$$

$$\phi_r = \mathrm{atan2}\left(-c_{\theta_r} s_{\phi_r} n_x + c_{\theta_r} c_{\psi_r} n_y, -n_z\right). \tag{51}$$

where g is the gravity constant and ψ_r is the yaw angle reference. We calculate the body frame values $\boldsymbol{\nu}_r$ using equation (7). A local minimum in the magnitude of the field can be noticed on Fig. 4. This is because of opposing virtual leader and collision avoidance force. The vehicles will not be caught in this minimum because it is not a stable minimum, unlike the desired position, see Fig. 4 (b).

3.5 Stability

It is advisable to limit the virtual leader influence. Due to the fact that a waypoint can be far away from the actual position, the field component in equation (35) respectively (36) can become large because of a large $\mathbf{d}_i$. This would result in a domination of the virtual leader part in the potential field and could constrict an effective collision or obstacle avoidance. Stability of the single vehicles is ensured by the underlying control system which is used to follow the vehicle's trajectories generated by the potential field. The used control system is discussed in [3].

Assumption 1 *It is assumed that stability of the overall formation system is guaranteed if the generated trajectories are feasible for the underlying control system (e.g. in causing limited control actions).*

The used controller requires a continuous trajectory which is provided by the presented solution. Other controllers may induce additional restrictions which need to be covered by adjusting the algorithm. We have found that varying $\mathrm{K_{vl}}$, and then choosing

$$\mathrm{K_{ij}} = \mathrm{K_{vl}}/\mathrm{N}, \tag{52}$$

$$\mathrm{K_{ca}} = 10 \cdot \mathrm{K_{vl}} \cdot r_{sav}^{min}, \tag{53}$$

where N represents the amount of vehicles in the group results in good performance. The numerical value of K_{v1} will vary from case to case. Due to the fact that the controller in Fig. 2 normally takes the reference velocity into account, r_{sav}^{min} should be chosen as the distance, the vehicle needs to perform a stop from full speed. Using the distances $\mathbf{d}_{i0}$ and $\mathbf{d}_{ij0}$ in (36) and (38) improves the robustness during flight by reducing necessary calculations or communications. The distance between virtual leader and vehicles remains constant, independent of the current swarm position. A continuous calculation and update of the desired position of each vehicle in the formation is not necessary while the virtual leader is moving.

4 Simulation results

In this section we present some simulations illustrating the approach. Fig. 5 shows an in flight formation reconfiguration. A group of three helicopters changes from line to triangle formation.

Fig. 5. Formation reconfiguration

Fig. 6. Vector 2-norm of the distance between the desired ($\mathbf{p}_r^n$) and current ($\mathbf{p}^n$) position of the vehicles in Fig. 5. Top graph for the red vehicle, middle graph for the green and lower graph for the blue one.

Fig 6 shows the corresponding vector 2-norm of the distance between desired and current position of the tree vehicles. This distance is equal to the individual field magnitude $||\mathbf{F}_i^{tot}||$ at the vehicles position. There are three interesting times:

(1) 36s: The vehicles begin to change from line to triangle formation. Introduced by reaching a waypoint.
(2) 52s: The vehicles reach an other waypoint, where they finish the formation reconfiguration.
(3) 53s: F_{max} is reached. The field magnitude continues to increase while the vehicles keep accelerating as discussed in connection with equation (46).

An appropriate mission for groups of small scale helicopter UAVs are power line inspections. In Fig. 7, a group of five helicopters is heading toward a power line. No adjustments of gains were necessary.

Fig. 7. Obstacle avoidance

As in Fig. 4 (a), the potential field has an unstable local minimum in front of the obstacle which is passed by the vehicles, see section 3.4. The autopilot of [3] was used. This is a cascade controller, controlling rotational movement in the

inner loop and translational movement in the outer loop. The parameters used for the presented simulations can be found in Table 1. More details regarding the autopilot and simulations can be found in [19].

Table 1
Potential field parameter

5 Conclusion

In this paper, we presented a solution for collision and obstacle free formation flight and reconfiguration of groups of autonomous helicopters. The solution is based on potential fields using a virtual leader and taking the vehicle's velocities into account. It is universal applicable using the vehicle's auto pilot. The formation flight solution works very well with the presented simplified helicopter model.

There are several topics for future work on this topic. Validation with complete models of other vertical take-off and landing (VTOL) UAVs could be useful. There might be a possibility for the individual components in (34) to be in conflict. A study of this could include automatic tuning of gains or weights for the different components. Another group of topics of interest could be to study how to employ the proposed method in the case of critical system failures such as engine problems, sensor failures or communication faults.

References

[1] G. Elkaim and R. Kelbley, "A lightweight formation control methodology for a swarm of non-holonomic vehicles," in *Aerospace Conference*, March 2006.

[2] K. D. Do, "Formation control of mobile agents using local potential functions," in *Proceedings of the American Control Conference*, June 2006.

[3] L. Marconi and R. Naldi, "Robust nonlinear control of a miniature helicopter for aerobatic maneuvers," in *Proceedings 32th Rotorcraft Forum*, September 2006.

[4] F. Xie, X. Zhang, R. Fierro, and M. Motter, "Autopilot-based nonlinear uav formation controller with extremum-seeking," in *Proceeding of the 44th IEEE Conference on Decision and Control*, 2005.

[5] L. Vig and J. A. Adams, "Multi-robot coalition formation," *IEEE Transactions on Robotics*, vol. 22, no. 4, pp. 637–649, August 2006.

[6] S. Waydo, J. Hauser, R. Bailey, E. Klavins and R. M. Murray, "UAV as a Reliable Wingman: A Flight Demonstration," *IEEE Transactions on Control Systems Technology*, vol. 15, no. 4, pp. 680–688, July 2007.

[7] D. Galzi and Y. Shtessel, "Uav formations control using high order sliding modes," in *Proceedings of the American Control Conference*, 2006, pp. 4249–4255.

[8] A. Restas, "Wildfire management supported by uav based air reconnaissance: Experiments and results at the szendro fire department, hungary," in *First International Workshop on Fire Management*, April 2006.

[9] S. Herwitz, S. Dunagan, D. Sullivan, R. Higgins, L. Johnson, J. Zheng, R. Slye, J. Brass, J. Leung, B. Gallmeyer, and M. Aoyagi, "Solar-powered uav mission for agricultural decision support," in *Proceedings of the IEEE International Geoscience and Remote Sensing Symposium*, vol. 3, July 2003, pp. 1692– 1694.

[10] G. D. Padfield, *Helicopter Flight Dynamics: The Theory and Application of Flying Qualities and Simulation Modelling*. Blackwell Science, 1996.

[11] R. K. Heffley and M. A. Mnich, "Minimum-complexity helicopter simulation math model," NASA, Tech. Rep. NAS2-11665, April 1988.

[12] V. Gavrilets, B. Mettler, and E. Feuron, "Nonlinear model for a small-sized acrobatic helicopter," in *AIAA Guidance, Navigation and Control Conferance*, no. AIAA 2001-4333. AIAA, August 2001.

[13] A. Bogdanov, E. Wan, and G. Harvey, "Sdre flight control for x-cell and r-max autonomous helicopters," in *43rd IEEE Conference on Decision and Control*, December 2004, pp. 1196 – 1203.

[14] I. I. Kaminer, O. A. Yakimenko, V. N. Dobrokhodov, M. I. Lizarraga and A. M. Pascoal, "Cooperative control of small UAVs for naval applications," in *43rd IEEE Conference on Decision and Control*, December 2004, pp. 626 – 631.

[15] B. Seanor, Y. Gu, M. R. Napolitano, G. Campa, S. Gururajan and L. Rowe, "3-Aircraft Formation Flight Experiment," in *Proceedings of the 14th Mediterranean Conference on Control and Automation*, June 2006.

[16] E. N. Johnson and S. Kannan, "Adaptive flight control for an autonomous unmanned helicopter," in *AIAA Guidance, Navigation and Control Conference*, no. AIAA-2002-4439, Monterey, CA, August 2002.

[17] T. I. Fossen, *Marine Control Systems - Guidance, Navigation, and Control of Ships, Rigs and Underwater Vehicles*. Marine Cybernetics, November 2002.

[18] V. Gavrilets, "Autonomous aerobatic maneuvering of miniature helicopters," Ph.D. dissertation, Massachusetts Institute of Technology, May 2003.

[19] T. Paul, "Reconfiguration in Formations of Unmanned Aerial Vehicles," MSc. Thesis, Technische Universität Darmstadt and Norges teknisk naturvitenskapelige universitet, April 2007.

Figure

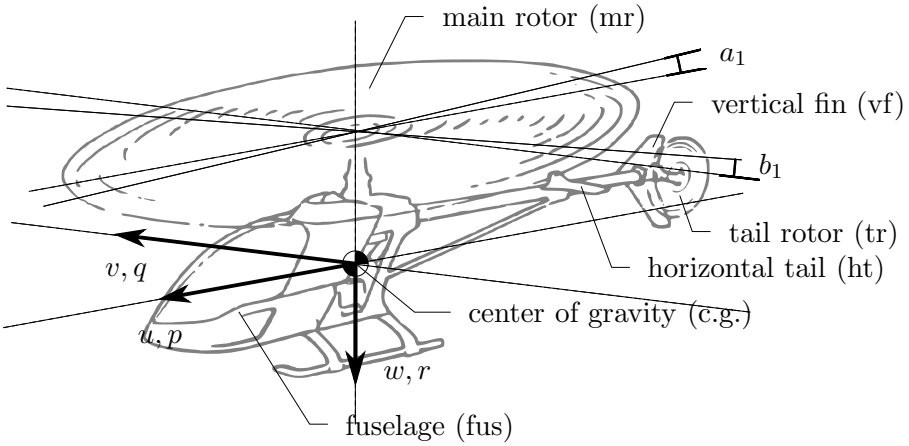

Fig.1 Body fixed frame and helicopter components

Figure

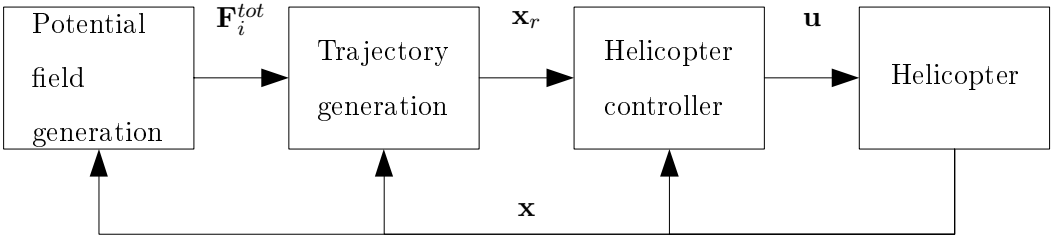

Fig.2 Vehicle block diagram

Figure

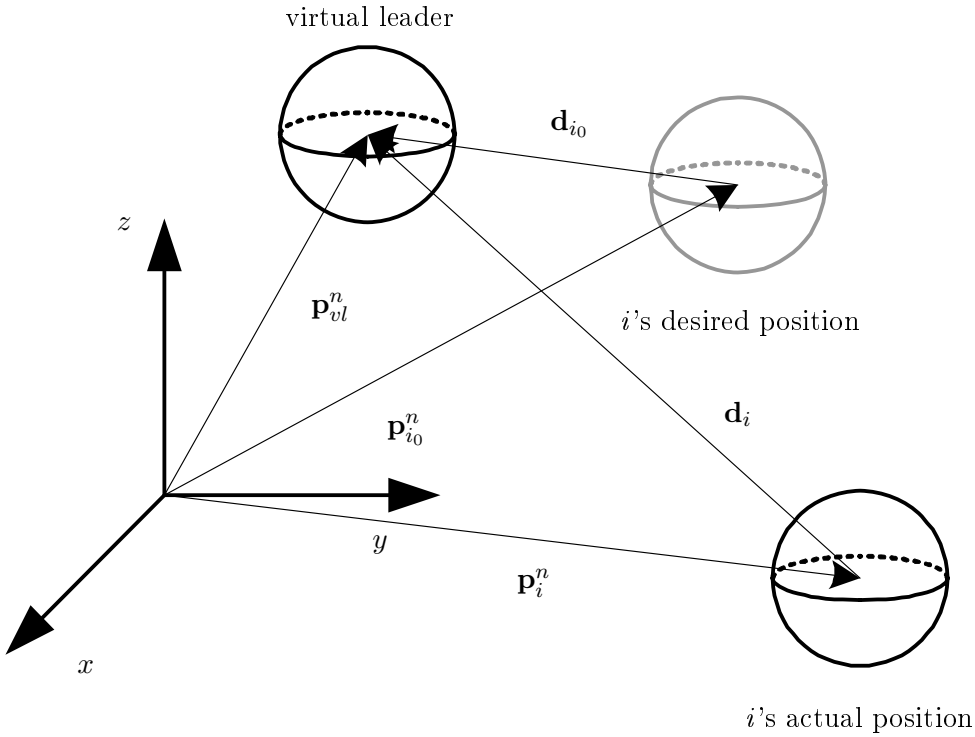

Fig.3 Vector definitions for formation flight; $\mathbf{p}_{vl}^n$: position vector of virtual leader; $\mathbf{p}_i^n$: current position vector of vehicle i; $\mathbf{p}_{i0}^n$: vehicle i's place in the formation

Figure

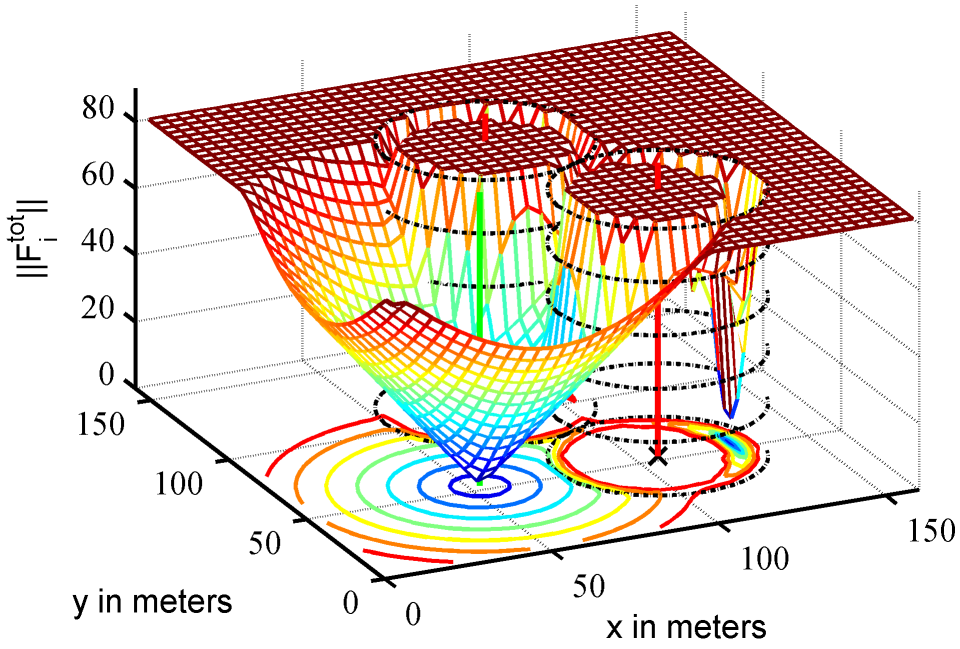

(a)

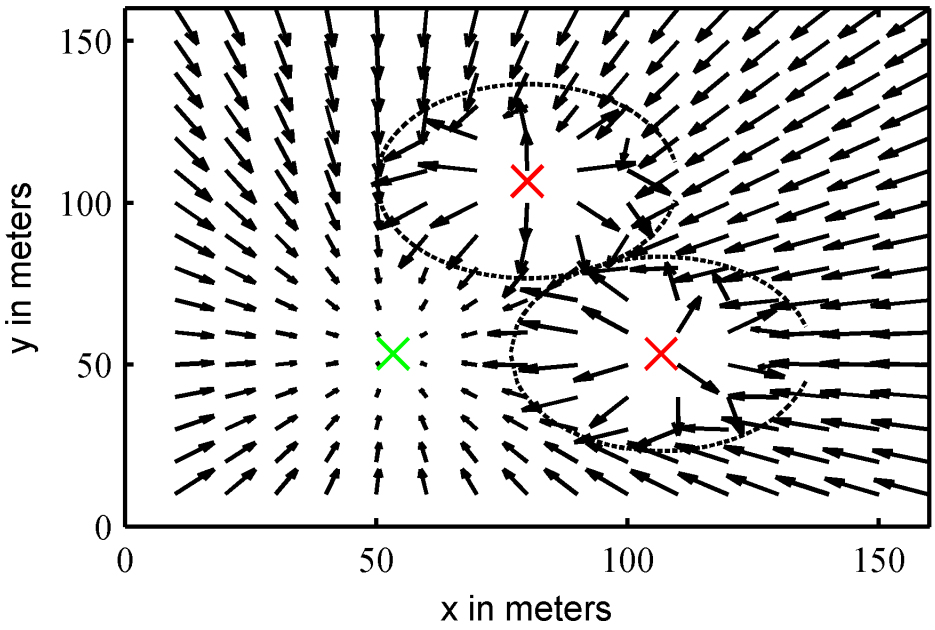

(b)

Fig.4 (a) Potential field magnitude (b) Potential field direction. The used r_{sav} is indicated by black circles and the vehicles position by the red (opponent) and green (desired) lines resp. crosses.

Figure

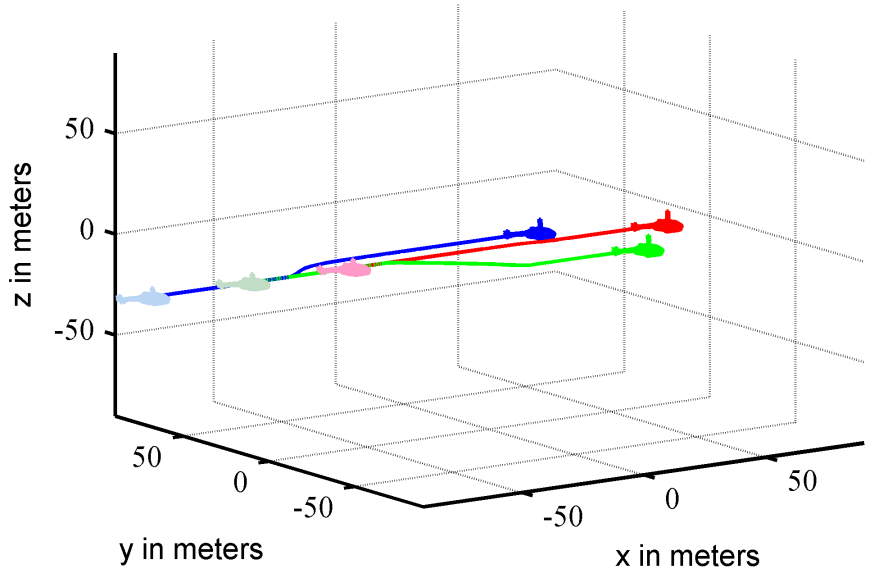

Fig.5 Formation reconfiguration

Figure

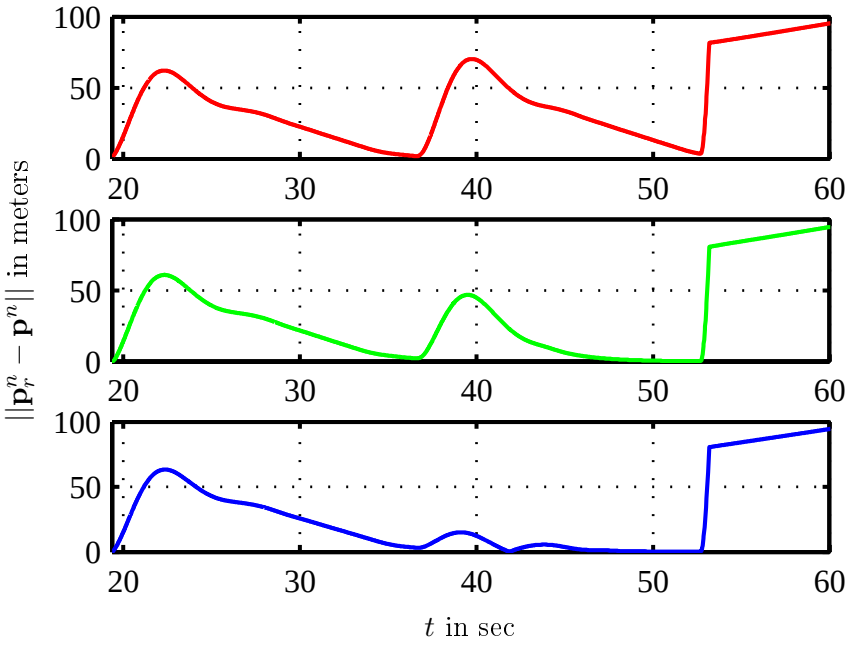

Fig.6 Vector 2-norm of the distance between the desired ($\mathbf{p}_r^n$) and current ($\mathbf{p}^n$) position of the vehicles in Fig. 5. Top graph for the red vehicle, middle graph for the green and lower graph for the blue one.

Figure

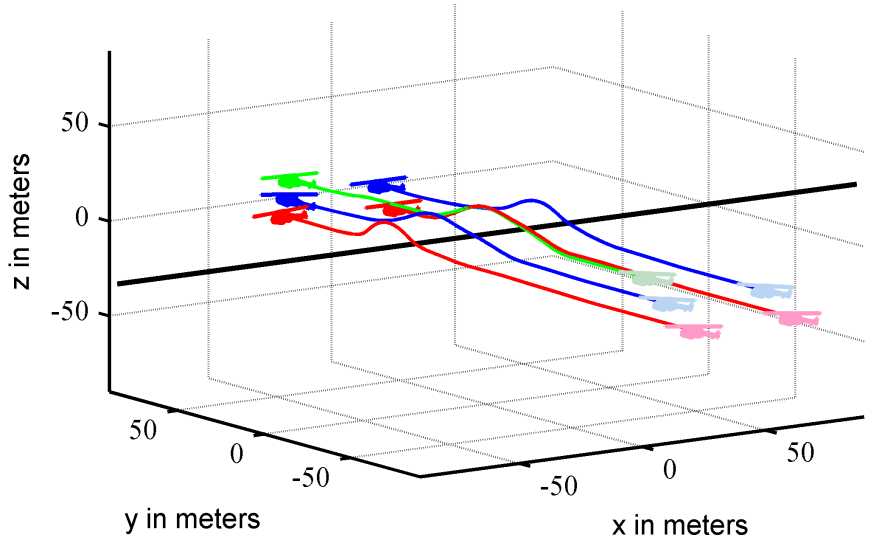

Fig.7 Obstacle avoidance

Table

Parameter	Description
$F_{max} = 80$	Maximum field strength
$F_{min} = 3$	Minimum field strength
$r_{sav}^{min} = 30m$	Safety radius
$K_{vl} = 1$	Virtual leader gain
$K_{iv} = 0.1$	Inter vehicle gain
$K_{ca} = 240$	collision avoidance gain

Table 1
Potential field parameter